PHOTONICS Research

Frequency-domain parametric downconversion for efficient broadened idler generation

YING LI, YUHAI LIANG, DAHUA DAI, JIANLONG YANG, HAIZHE ZHONG,* AND DIANYUAN FAN

International Collaborative Laboratory of 2D Materials for Optoelectronic Science & Technology of Ministry of Education, Engineering Technology Research Center for 2D Material Information Function Devices and Systems of Guangdong Province, College of Optoelectronic Engineering, Shenzhen University, Shenzhen 518060, China
**Corresponding author: haizhe.zhong@szu.edu.cn*

Received 4 September 2017; revised 11 October 2017; accepted 11 October 2017; posted 12 October 2017 (Doc. ID 306467); published 7 November 2017

An opposite-chirped frequency-domain optical parametric amplification (OC-FOPA) design is demonstrated and numerically verified. This scheme combines both an ultrabroad seeding generation and the subsequent effective amplification in one single optical parametric amplification stage. Based on a slightly asymmetrical 4-*f* optical system, the spectral contents of both pump and signal waves are spectrally dispersed with opposite spatial chirps, to broaden the initial idler seeding. Via a properly designed fan-out periodically poled $LiNbO_3$ chip, nearly perfect quasi phase matching can be realized across the full spectrum, whereby each individual spectral pair precisely maps to its required grating period. Full-dimensional simulations based on commercial ~110 fs (FWHM) near-infrared (near-IR) lasers at 790 and 1030 nm are quantitatively discussed, and few-cycle mid-IR laser pulses (~60 fs at 3.4 μm) plus a high conversion efficiency exceeding 50% are theoretically predicted. By means of a high-power pump source, the OC-FOPA scheme can be also applied to directly produce high-intensity carrier-envelope-phase-stabilized mid-IR idler pulses.

OCIS codes: (190.4970) Parametric oscillators and amplifiers; (320.7110) Ultrafast nonlinear optics; (320.7160) Ultrafast technology.

https://doi.org/10.1364/PRJ.5.000669

1. INTRODUCTION

Few-cycle mid-infrared (mid-IR) ultrafast laser sources are of great interest for a diverse range of applications from high harmonic generation [1,2] and laser wakefield acceleration [3,4] to spectroscopic investigation [5]. Exponentially increased efforts in the development of higher-intensity mid-IR lasers have been undertaken over the last 10 years [6–10], among which nonlinear downconversion is the common method for generating intensive mid-IR lasers that are not easily accessible with a mode-locked laser. In particular, broadband difference-frequency generation (DFG) or optical parametric amplification (OPA) between two conventional near-IR laser sources has been widely exploited for few-cycle mid-IR pulse generation, as the idler wave [11–13]. Generally, it rests upon two inevitable ingredients: an ultrabroad driving laser for seeding generation and the subsequent ultrabroad OPA stages for energy boosting [14]. First, the original bandwidth of the mid-IR seeding is primarily determined by the driving laser. Usually, to meet this ultrabroad bandwidth requirement, the driving laser should have been previously spectrally broadened via continuum generation in various nonlinear media [15–17] or filamentation in gases [18,19]. For the subsequent broadband OPA stages, then, a sufficiently broad parametric gain spectrum, which determines the amplification ability on the potential shortest pulse duration, is the other critical issue. To ensure the effective amplification of few-cycle laser pulses, strategies such as postcompression in hollow-core fiber [20,21], noncollinear optical parametric chirped pulse amplification (OPCPA) [22–24], or, as demonstrated in Refs. [25,26], frequency-domain OPA (FOPA) have been proposed.

In this paper, we present and numerically verify an opposite-chirped FOPA (OC-FOPA) scheme capable of high-power ultrafast mid-IR pulse generation. Here, with a slightly asymmetric 4-*f* optical system, broadband pump and signal pulses are oppositely spatial chirped. The opposite instantaneous frequency deviations of the signal and pump beams enable the initially generated idler pulse to have a significantly broader spectrum than those of the driving pulses. To realize perfect phase matching (PM) across such a broad spectrum region, periodically poled $LiNbO_3$ (PPLN) crystal with a fan-out grating structure is adopted as the nonlinear medium. As long as the spatially varying grating period of $\Lambda(x)$ is appropriately designed, quasi PM (QPM) and the consequent efficient parametric amplification can be realized for each individual spectral

pair. The proposed OC-FOPA scheme handily combines both ultrabroad mid-IR seeding generation and the subsequent effective amplification in one single OPA stage. In theory, without the help of previous spectrum broadening or postcompression, few-cycle mid-IR laser pulses can be efficiently generated via a common commercial ~110 fs near-IR driving laser.

2. CONCEPT OF THE OC-FOPA SCHEME

Nonlinear downconversion is a well-established laser technology for filling mid-IR spectral gaps or enhancing the laser energy at any wavelength of interest, termed DFG or OPA. In a standard ultrafast OPA device, the pump and signal pulses are both nearly transform limited (TL) with femtosecond pulse durations [27,28]. The ubiquitous group velocity mismatch (GVM) thus has a determinative effect on limiting the effective interaction length and narrowing the gain bandwidth [29,30]. Although enhancing the pump intensity can make up for this insufficient nonlinear interaction, the maximum pump intensity is still limited by the damage threshold of crystal. To scale up the pumping energy, the well-known OPCPA design was proposed. Recently, Zhang *et al.* reported an OPA scheme called dual-chirp OPA (DC-OPA) [31,32]. Unlike conventional OPCPA cases, in this scheme, temporally chirped broadband pump pulses are employed. By properly managing the temporal chirps, PM can be achieved for each individual temporal slice of the pump and signal pulses, allowing the use of a longer crystal without either gain narrowing or efficiency loss. In addition, compared with the OPCPA scheme, DC-OPA has more degrees of freedom to control the spectral characteristic of the idler wave. Specifically, when the chirp signs of the pump and signal pulses are opposite, an initial idler pulse with a remarkably broadened spectrum compared with those of the driving pulses is expected. However, the shortest idler pulse we can obtain is still limited by the acceptable PM bandwidth of the nonlinear crystal. Unfortunately, opposite chirp signs normally provide more rigorous PM conditions [33]. The restricted PM bandwidth, in combination with the temporally varying intensity envelope, makes it more difficult to tackle the gain narrowing in the opposite DC-OPA systems. Phase-matched amplification over such an ultrabroad spectrum is still challenging. FOPA was first proposed by Schmidt *et al.*, and is capable of simultaneous upscaling of peak power and amplified spectral bandwidth [26]. In this scheme, a signal beam is spectrally dispersed in the Fourier plane, and then the broad spectrum can be amplified "slice by slice." Several individual nonlinear crystals are used to broaden the gain spectrum, where each is tuned for optimal amplification of its corresponding spectral slice. Then, a two-dimensionally patterned QPM medium is introduced for gain-spectrum tailoring and to relax the influence of the sharp crystal edges [25].

On the basis of the FOPA scheme, we propose a different strategy for high-power ultrafast mid-IR pulse generation that combines both ultrabroad seeding generation and efficient parametric amplification in one single OPA stage. The proposed OC-FOPA scheme is conceptually illustrated in Fig. 1, in which a slightly asymmetric 4-f optical system is employed. In this setup, various frequency components of signal and pump pulses are separately spectrally distributed in space. As

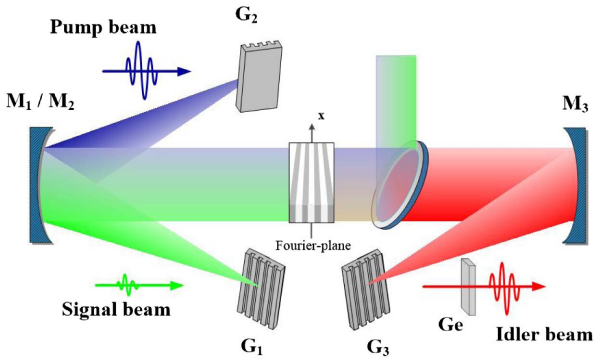

Fig. 1. Schematic illustration of the proposed OC-FOPA scheme.

shown, the signal and pump pulses pass through the sequent diffraction grating G_1/G_2 and collimating mirror M_1/M_2 individually. Then, each frequency component spectrally distributes and focuses into its separate focus in the Fourier plane. To broaden the initially generated idler spectrum, the expanded pump and signal beams overlap with opposite linear spatial chirps. To realize the optimum OPA throughout the ultrabroad idler spectrum, a single monolithic QPM crystal with a fan-out profile is employed, whose spatially varying grating period $\Lambda(x)$ exactly phase matches to the inhomogeneous QPM condition of $|k_p(x) - k_s(x) - k_i(x)| = 2\pi/\Lambda(x)$. Perfect PM thus can be achieved across the entire chirped beams. After the efficient nonlinear downconversion, optical Fourier transformation of the amplified idler wave is carried out from the frequency domain to the temporal domain, while the amplified signal and the residual pump beams are both filtered via a dichroic mirror. Finally, ultrafast idler pulses are obtained after necessary dispersion compensation.

In the Fourier plane, the instantaneous angular frequency of idler can be regarded as the algebraic subtraction between those of the signal and pump pulses. Supposing the signal and pump pulses have an equal bandwidth of $\Delta\omega$ and an equal initial beam radius, the generated idler bandwidth will be doubled, and then the spatial chirp $(\partial x/\partial \nu)$ gets only one half of the original when both beams are chirp expanded to a same size. Thus, after a conventional 4-f optical propagation, the idler angular dispersion to be compensated would also be just one half of that the incident gratings provided. In addition to distinct operation wavelengths, the angular dispersions should also be remarkably different for the gratings in the input and output ends, resulting in a slightly asymmetric 4-f setup.

3. PROOF OF PRINCIPLE

Under an assumption that the collimating mirrors employed have a long focal length, and the focusing and diffraction effects are ignorable, the temporal–spatial coupled beams in the Fourier plane can be approximately described as [34]

$$A(x,y,t) = b\,\exp\left\{-\left[\frac{x^2}{(1+u)\sigma^2}+\frac{y^2}{\sigma^2}\right]+\left[-\frac{t^2}{\tau_0^2(1+u)}\right]\right\} \times \exp\left[-i\frac{2\sqrt{u}xt}{(1+u)\sigma\tau_0}\right], \quad (1)$$

Table 1. Nonlinear Optical Crystal Parameters for 5% Doped MgO:PPLN at 24.5°C ($\lambda_p = 790$ nm, $\lambda_s = 1030$ nm, $\lambda_i = 3.4$ μm)

d_{eff} (pm/V)	ν_{pump} (m/s)	ν_{signal} (m/s)	ν_{idler} (m/s)	Λ_0 (μm)	GVD_{pump} (fs^2/mm)	$\text{GVD}_{\text{siganl}}$ (fs^2/mm)	$\text{GVD}_{\text{idler}}$ (fs^2/mm)
16	$c/2.258$	$c/2.207$	$c/2.203$	21.9	367	246	−800

where σ and τ_0 respectively present the beam radius and the initial pulse duration in half-width at $1/e^2$ maximum of the radial intensity distribution. The last exponential function states the linear frequency sweep across the x axis. Clearly, due to this spatial chirp, for each focal spot in the Fourier plane, the spectral variation is orders of magnitude smaller and the pulse duration is stretched correspondingly to be $\tau_0(1+u)^{1/2}$. Here, $(1+u)^{1/2}$ is defined as the spatial chirp coefficient, which is also the ratio between the major and minor axes of the chirp-expanded beam.

To demonstrate the optimized performance of the proposed configuration, focusing on the conversion efficiency and the idler spectrum bandwidth, a typical OPA process between 790 and 1030 nm femtosecond pulses was numerically studied, in which the desired mid-IR pulses at ~3.4 μm were concomitantly generated as the idler wave [35]. A conventional femtosecond OPA (fs-OPA) scheme was also considered for comparison. A 5% MgO-doped PPLN crystal, which is widely adopted for mid-IR laser generation, was used [36]. Interacting waves were all e-polarized so that the largest d_{33} nonlinear coefficient could be utilized. Full-dimensional (x, t, z) simulations were conducted based on the well-known nonlinear coupled-wave equations numerically solved by a standard split-step method [23]. The essential parameters, calculated based on the temperature-dependent Sellmeier equations for 5% doped MgO:PPLN [37], are summarized in Table 1. In our simulations, temporal dispersion terms of GVM and group velocity dispersion (GVD) were both taken into account, while the diffraction effect was ignored. Figures 2(a) and 2(b) present the simulated small-signal dependence of conversion efficiency and spectrum bandwidth of the generated mid-IR idler pulses on the crystal length. The nonlinear length L_{nl}, which is a measure of the pump intensity or parametric gain, is presented correspondingly [38]. The pump and signal pulses possess an equivalent initial temporal duration τ_0 of 100 fs. For the OC-FOPA scheme presented, the spatial chirp coefficient $(1+u)^{1/2}$ was set to be 100. At each focal spot, consequently, both the signal and pump pulses were temporally stretched from 100 fs to 10 ps with opposite chirp signs. It should be noted that normally, damage fluence scales with the root square of pulse duration [39]. Thus, the driving intensity used here is only one tenth of that used in the fs-OPA situation. Meanwhile, the crystal length gets $10^{1/2}$ longer to compensate the reduced intensity and ensure a uniform gain when GVM effects are negligible. Since a sufficiently broad original spectrum is the prerequisite for obtaining broadband pulses after amplification, we pay attention first to the initial bandwidth of the idler pulses. As is shown in Fig. 2(c), for the fs-OPA scheme, the initial idler spectrum is obviously wider than the initial spectrum of the driving pulses ascribed to the frequency mixing of various frequency components. Despite the lack of frequency mixing, by virtue of the opposite spatial chirps, the OC-FOPA scheme is also able to overcome the gain narrowing resulting from the nonuniform spectral gain, and obtains a broadened idler output [shown in Fig. 2(d)].

As the crystal length increases, however, although the spectral bandwidth is almost untouched, the conversion efficiency shows a significant decrease for the conventional fs-OPA cases, caused by the more prominent GVM effects. As for the OC-FOPA scheme, besides the fan-out PPLN design, a simpler PPLN chip with a unique grating period was also considered. However, although the stretched pluses significantly relieved the GVM effects on pulse slipping, contradiction between the limited gain bandwidth and such a broad idler spectra is another stumbling block, resulting in a synchronous dropping of the overall conversion efficiency and the idler spectral bandwidth [dashed lines in Fig. 2(b)]. In comparison, the broadened mid-IR seeding can be efficiently amplified without loss of any spectral bandwidth as long as an optimized fan-out PPLN crystal is adopted [solid lines in Fig. 2(b)].

Obviously, the spectral bandwidth of the idler strongly depends on the transverse grating varying of the nonlinear crystal. For the linearly chirped fan-out PPLN chips, the grating period $\Lambda(x)$ is a function of transversal location x, which can be expressed as $\Lambda(x) = \Lambda_0 + \kappa'(x - x_0)$, where κ' is the grating chirp rate. Λ_0 represents the grating period in the cross section center. Here, Λ_0 is always chosen to ensure QPM for the center wavelengths. If the GVM effects are negligible, then the interacting waves are quasi-continuous at each focal spot.

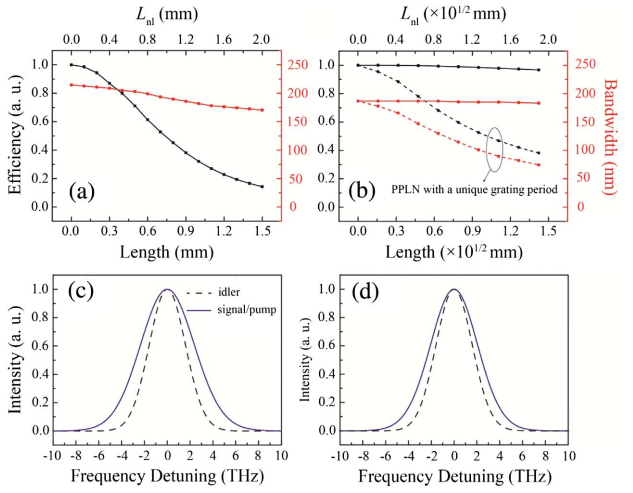

Fig. 2. Simulated dependence of conversion efficiency and spectrum bandwidth of the mid-IR idler pulses on the crystal length, for (a), (c) the conventional fs-OPA and (b), (d) the proposed OC-FOPA schemes. It should be noted that for all intensity–length pairs of each OPA scheme, constant conversion efficiency and a similar idler spectrum [(c), (d)] can be achieved in the absence of temporal pulse slipping. The initial signal intensity was fixed at 1% of the pump intensity.

Figures 3(a) and 3(b) presents the small-signal idler spectrum bandwidth versus various grating chirp rates for different pulse duration pairs. It's clear that for each duration case, there is a specialized grating chirp rate where the idler spectrum is the broadest. Obviously, there is an explicit one-to-one correlation between the optimum chirp rate and the instantaneous frequency pairs. For the fixed spectrally expanded beam profiles, the spectrum bandwidth of each individual pulse determines its spatial chirp ($\partial x/\partial \nu$) in the Fourier plane, and thus the overlap of each instantaneous frequency pair.

Likewise, for a specific nonlinear parametric process, the optimum chirp rate can also be adjusted by manipulating the spectrally expanded beam profiles. The $(1+u)^{1/2}$-dependent optimum chirp rates are presented in the insets of Figs. 3(a) and 3(b), under the abovementioned operation conditions. As is shown, the optimum chirp rate reveals an approximate inverse proportional relationship to the spatial chirp coefficient of $(1+u)^{1/2}$. As long as proper spatial chirps are chosen, in theory, the optimum gain spectrum can always be achieved via a pre-existing fan-out design, even for various pulse duration cases. This actually facilitates the implementation of the proposed scheme, and relaxes the precise design and fabrication of distinct specified fan-out profiles. Spectrum details near the maximum idler bandwidth are given in Figs. 3(c) and 3(d). As can be seen, in the vicinity of the peak value, idler spectra show obvious redshifting or blueshifting with respect to the right and left sides of the optimum result. In the paper, only a relatively simple linear design was discussed. For extremely broadband frequency conversions, flat gain spectra can be obtained through the use of a nonlinearly chirped QPM grating.

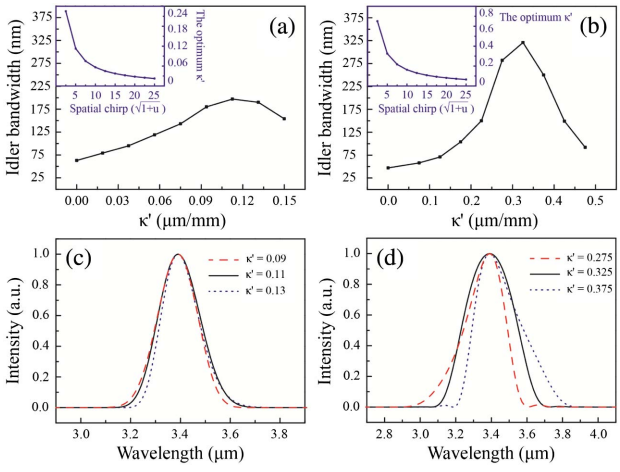

Fig. 3. (a), (b) Small-signal idler spectrum bandwidth versus various grating chirp rates and (c), (d) spectrum details near the maximum value with a fixed spatial chirp coefficient $(1+u)^{1/2}$ of 5, for different pulse duration cases. In the calculations, pump and signal have equivalent elliptical beam profiles, and the major and minor axes are 5 and 1 mm, respectively. The PPLN crystal length is fixed at 5 mm. Insets: The $(1+u)^{1/2}$-dependent optimum chirp rates. τ_{pump} and τ_{signal} represent the pulse duration of the pump and signal pulses, respectively. (a), (c) $\tau_{pump} = 35$ fs and $\tau_{signal} = 100$ fs; (b), (d) $\tau_{pump} = 100$ fs and $\tau_{signal} = 100$ fs.

4. INFLUENCE OF THE GVM EFFECTS

For the conventional fs-OPA device, GVM plays a critical role in limiting the effective interaction length. In the proposed OC-FOPA scheme, the broadband interacting waves are spatially chirped in the Fourier plane, resulting in linearly divided spectrum components and an accordingly stretched pulse duration. Parametric amplification in the frequency domain not only provides the possibility of broadband PM, the stretched pulse duration, but also essentially weakens the detrimental GVM effects. However, pulse slipping still occurs as long as the interacting pulses are not sufficiently spatially chirped.

In this section, we draw attention to the GVM effects on both the parametric gain and the peculiarities of the idler beam. In our simulations, the pump and signal waves had the same beam radius and TL pulse duration ($\tau_0 = 100$ fs, i.e., ~110 fs at FWHM). A 5 mm fan-out PPLN crystal was employed, and the optimum grating chirp rates were always chosen. The initial signal intensity was 1% of the pump intensity, while the pump intensity was fixed at ~240 MW/cm^2, which was selected to drive the OC-FOPA to saturation without the occurrence of back-conversion. Ignoring the influence of material dispersion, an ideal quantum conversion efficiency of ~70% was predicted in the beam center, and the overall efficiency was about 50%. Clearly, by virtue of the reduced pulse slipping, the conversion efficiency monotonically increases to its ideal limit as the spatial chirp coefficient increases [shown in Fig. 4(a)]. Nevertheless, the temporal and spectral characteristics of the idler wave seem nearly insensitive to the GVM effects, so that a stable spectrum and pulse envelope outputs are always obtained [shown in Figs. 4(c)–4(f)]. Figure 4(b) presents the amplified idler spectra and the dispersion-compensated pulse envelopes. As shown,

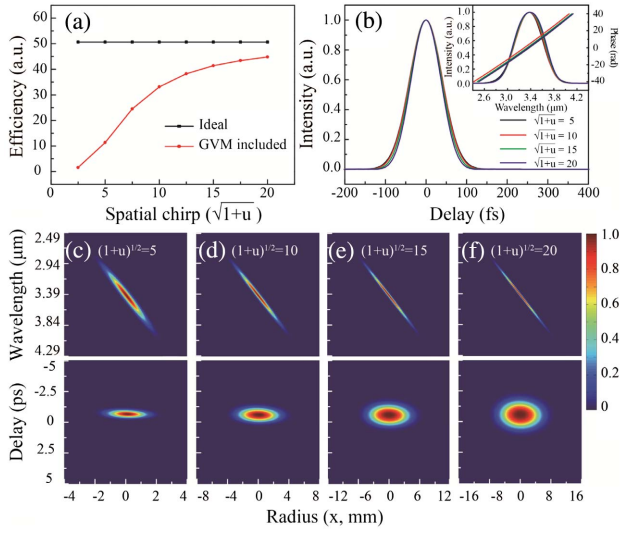

Fig. 4. (a) Dependence of the photon conversion efficiency on the spatial chirp coefficient $(1+u)^{1/2}$, (b) the amplified idler spectra and the corresponding dispersion-compensated pulse envelopes, (c)–(f) the individual extracted spatial–spectral and spatial–temporal profiles. In the calculations, pump and signal have equivalent elliptical beam profiles, and the minor axes are fixed at 1 mm for various spatial chirp coefficients. The idler spectrum is obtained by linear superposition of each individual spectrum component across the spatial chirp axis x.

similar spectrum profiles are theoretically predicted, showing an ultrabroad bandwidth exceeding 500 nm and a corresponding ~90 fs recompressed pulse duration at FWHM, which is ~20% shorter than those of the driving lasers. This intriguing feature may be caused by the independent frequency amplification processes. Various frequency contents linearly distributed in the Fourier plane and the perfect QPM can be achieved across nearly the whole idler spectrum by means of the optimum grating structure. In a weak spatial chirp situation, although the interacting waves no longer are termed as quasi-continuous and pulse slipping still exists, the center frequency at each spot dominates the nonlinear process and obtains the most effective amplification since of the perfect QPM and its highest driving intensity. As a result, it is the fan-out profile and the consequent gain spectrum that determine the amplified idler spectrum. The temporal walk-off can only reduce the effective length and the conversion efficiency in turn, but gives rise to obvious spectrum distortion of the idler wave. In comparison, remarkable pulse envelope distortion derived from the pulse slipping is generally a major concern in conventional OPA devices [40,41]. This beneficial characteristic enables high-quality broadband idler pulses to be generated even in weak spatial chirp situations.

5. PULSE CHARACTERIZATION AND DISCUSSION

Finally, the spectrum evolution of the 3.4 μm idler wave is explored for a detailed investigation. The incident pump intensity is fixed at 240 MW/cm^2 while the signal intensity varies from 0.1% of the pump intensity up to 10%. The amplified idler spectra and the dispersion-compensated pulse envelopes at different seeding intensities are respectively presented in Figs. 5(a) and 5(b). By virtue of the frequency domain amplification, the spatially distributed frequency components show nearly independent developments. The idler spectrum keeps broadening as the seeding intensity increases, as a result of the prior gain saturation in its central part. Eventually, the idler spectrum becomes near-super-Gaussian with a spectrum dip in the vicinity of the central wavelength. Clearly, in cases of OPCPA or the OC-FOPA presented, matching the pulse duration of pump and signal waves to reach the highest efficiency might also reduce the gain bandwidth, simply because of the lower pump intensity in the pulse tails. There is always a trade-off between the highest gain and the broadest bandwidth. To some extent, a moderate back-conversion may broaden the bandwidth of the idler pulse and thus result in a shorter pulse duration. As presented, the shortest pulse duration appears (~60 fs, which corresponds to only six cycles for a 3.4 μm carrier wavelength) when the spectral contents in the wings get sufficiently amplified, at the cost of a moderate back-conversion in the central part [dashed lines in Fig. 5(a)]. At the same time, a high conversion efficiency exceeding 50% is simultaneously obtained. However, the idler spectrum may suffer strong modulation if the seeding intensity is far beyond the saturation position, leading to multiple satellite pulses in the temporal domain [solid lines in Fig. 5(a)] [31]. In addition to controlling the spatial intensity profiles, we can also resort to a two-dimensionally patterned QPM medium to tailor the gain spectrum and obtain a flat spectrum output.

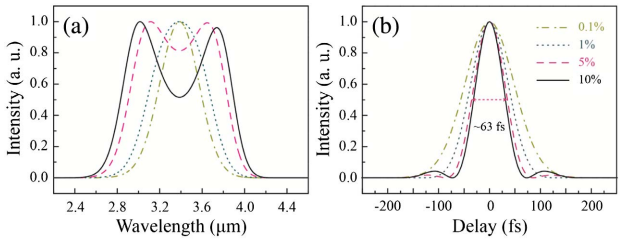

Fig. 5. (a) Amplified idler spectra and (b) dispersion-compensated pulse envelopes at different seeding intensities. To minimize the GVM effects, the spatial chirp coefficient $(1+u)^{1/2}$ was fixed at 20. The same simulation parameters were employed as those given in Fig. 4. The seeding intensity was set to 0.1%, 1%, 5%, and 10% of the pump intensity, corresponding to an overall efficiency of 9%, 50%, 59%, and 54%, respectively.

It should be noted that the driving lasers are only ~110 fs. The OC-FOPA scheme presented exerts a predominant effort on broadening the generated idler spectrum and the subsequent ultrabroad amplification. In recent years, large-aperture PPLN samples have been available [42]. In combination with new developments in high-power ultrafast amplifiers, this scheme should enable high-power and few-cycle pulse generation in mid-IR and even the terahertz regions.

In principle, synchronous signal and pump waves can be obtained from two separate femtosecond lasers, or the dual-wavelength outputs derived from a single driving laser. Compared with active carrier-envelope phase (CEP) stabilization, difference frequency mixing is favorable for passive stabilization of the CEP of idler pulses [43,44]. Provided that the pump and signal pulses originating from the same laser device possess analogous carrier phases, high-intensity self-CEP-stabilized mid-IR idler pulses can be directly produced. Furthermore, by virtue of semiconductor materials such as GaSe or periodic GaAs, the proposed OC-FOPA scheme can be also applicable to generating phase-locked few-cycle terahertz transients, when conventional oxide crystals exhibit strong absorption [45,46].

6. CONCLUSION

In conclusion, we have proposed and numerically verified an OC-FOPA scheme capable of both broadened idler seeding generation and ultrabroadband PM in a single monolithic QPM crystal. The spectral contents of both pump and signal waves are spectrally dispersed with opposite chirp signs via a properly designed fan-out PPLN chip, and nearly perfect QPM can be realized across the entire interacting beam profiles, whereby each individual spectral pair precisely maps to its required grating period. In such optimal cases, the amplified idler spectrum is insensitive to the GVM effects, so that stable spectrum and pulse envelope outputs are always obtained. A mild back-conversion in the vicinity of the central wavelength may help in broadening the idler spectrum and thus obtaining a shorter pulse duration. In theory, a commercial ~110 fs (FWHM) near-IR laser source is capable of generating few-cycle mid-IR laser pulses (~60 fs at 3.4 μm) with a high conversion efficiency exceeding 50%. To overcome the detrimental

gain narrowing resulting from the nonuniform pump intensity, in addition to controlling the spatial intensity profiles, we can resort to a two-dimensionally patterned QPM medium to obtain a more flat spectrum output. Furthermore, this scheme can also be applied to produce high-intensity self-CEP-stabilized idler pulses.

Funding. National Natural Science Foundation of China (NSFC) (61505113); Natural Science Foundation of Guangxi Province (2014A030310009); China Postdoctoral Science Foundation (2016M592527); Science and Technology Project of Shenzhen (JCYJ20160308091733202); Science and Technology Planning Project of Guangdong (2016B050501005); Educational Commission of Guangdong Province (2016KCXTD006).

REFERENCES

1. T. Popmintchev, M. C. Chen, D. Popmintchev, P. Arpin, S. Brown, S. Ališauskas, G. Andriukaitis, T. Balčiunas, O. D. Mücke, A. Pugzlys, A. Baltuška, B. Shim, S. E. Schrauth, A. Gaeta, C. Hernández-García, L. Plaja, A. Becker, A. Jaron-Becker, M. M. Murnane, and H. C. Kapteyn, "Bright coherent ultrahigh harmonics in the keV x-ray regime from mid-infrared femtosecond lasers," Science **336**, 1287–1291 (2012).
2. J. Weisshaupt, V. Juvé, M. Holtz, S. Ku, M. Woerner, T. Elsaesser, S. Ališauskas, A. Pugžlys, and A. Baltuška, "High-brightness table-top hard x-ray source driven by sub-100-femtosecond mid-infrared pulses," Nat. Photonics **8**, 927–930 (2014).
3. G. B. Zhang, N. A. M. Hafz, Y. Y. Ma, L. J. Qian, F. Q. Shao, and Z. M. Sheng, "Laser wakefield acceleration using mid-infrared laser pulses," Chin. Phys. Lett. **33**, 095202 (2016).
4. E. Esarey, C. B. Schroeder, and W. P. Leemans, "Physics of laser-driven plasma-based electron accelerators," Rev. Mod. Phys. **81**, 1229–1285 (2009).
5. C. Calabrese, A. M. Stingel, L. Shen, and P. B. Petersen, "Ultrafast continuum mid-infrared spectroscopy: probing the entire vibrational spectrum in a single laser shot with femtosecond time resolution," Opt. Lett. **37**, 2265–2267 (2012).
6. A. Hugi, G. Villares, S. Blaser, H. C. Liu, and J. Faist, "Mid-infrared frequency comb based on a quantum cascade laser," Nature **492**, 229–233 (2012).
7. Z. Qin, G. Xie, C. Zhao, S. Wen, P. Yuan, and L. Qian, "Mid-infrared mode-locked pulse generation with multilayer black phosphorus as saturable absorber," Opt. Lett. **41**, 56–59 (2016).
8. C. Y. Wang, T. Herr, P. Del'Haye, A. Schliesser, J. Hofer, R. Holzwarth, T. W. Hänsch, N. Picqué, and T. J. Kippenberg, "Mid-infrared optical frequency combs at 2.5 μm based on crystalline microresonators," Nat. Commun. **4**, 1345 (2013).
9. V. Shumakova, P. Malevich, S. Alisauskas, A. Voronin, A. M. Zheltikov, D. Faccio, D. Kartashov, A. Baltuska, and A. Pugzlys, "Multi-millijoule few-cycle mid-infrared pulses through nonlinear self-compression in bulk," Nat. Commun. **7**, 12877 (2016).
10. G. Andriukaitis, T. Balciunas, S. Alisauskas, A. Pugzlys, A. Baltuska, T. Popmintchev, M.-C. Chen, M. M. Murnane, and H. C. Kapteyn, "90 GW peak power few-cycle mid-infrared pulses from an optical parametric amplifier," Opt. Lett. **36**, 2755–2757 (2011).
11. I. Pupeza, D. Sánchez, J. Zhang, N. Lilienfein, M. Seidel, N. Karpowicz, T. Paasch-Colberg, I. Znakovskaya, M. Pescher, W. Schweinberger, V. Pervak, E. Fill, O. Pronin, Z. Wei, F. Krausz, A. Apolonski, and J. Biegert, "High-power sub-two-cycle mid-infrared pulses at 100 MHz repetition rate," Nat. Photonics **9**, 721–724 (2015).
12. S. C. Kumar, A. Esteban-Martin, T. Ideguchi, M. Yan, S. Holzner, T. W. Hansch, N. Picque, and M. Ebrahim-Zadeh, "Few-cycle, broadband, mid-infrared optical parametric oscillator pumped by a 20-fs Ti:sapphire laser," Laser Photon. Rev. **8**, L86–L91 (2014).
13. A. Thai, M. Hemmer, P. K. Bates, O. Chalus, and J. Biegert, "Sub-250-mrad, passively carrier-envelope-phase-stable mid-infrared OPCPA source at high repetition rate," Opt. Lett. **36**, 3918–3920 (2011).
14. G. Ernotte, P. Lassonde, F. Legare, and B. E. Schmidt, "Frequency domain tailoring for intra-pulse frequency mixing," Opt. Express **24**, 24225–24231 (2016).
15. K. Yin, B. Zhang, J. Yao, L. Yang, S. Chen, and J. Hou, "Highly stable, monolithic, single-mode mid-infrared supercontinuum source based on low-loss fusion spliced silica and fluoride fibers," Opt. Lett. **41**, 946–949 (2016).
16. C. H. Lu, Y. J. Tsou, H. Y. Chen, B. H. Chen, Y. C. Cheng, S. D. Yang, M. C. Chen, C. C. Hsu, and A. H. Kung, "Generation of intense supercontinuum in condensed media," Optica **1**, 400–406 (2014).
17. W. Yang, B. Zhang, G. Xue, K. Yin, and J. Hou, "Thirteen watt all-fiber mid-infrared supercontinuum generation in a single mode ZBLAN fiber pumped by a 2 μm MOPA system," Opt. Lett. **39**, 1849–1852 (2014).
18. A. V. Mitrofanov, A. A. Voronin, D. A. Sidorov-Biryukov, S. I. Mitryukovsky, A. B. Fedotov, E. E. Serebryannikov, D. V. Meshchankin, V. Shumakova, S. Ališauskas, A. Pugžlys, V. Ya. Panchenko, A. Baltuška, and A. M. Zheltikov, "Subterawatt few-cycle mid-infrared pulses from a single filament," Optica **3**, 299–302 (2016).
19. B. Shim, S. E. Schrauth, and A. L. Gaeta, "Filamentation in air with ultrashort mid-infrared pulses," Opt. Express **19**, 9118–9126 (2011).
20. S. Hadrich, H. Carstens, J. Rothhardt, J. Limpert, and A. Tunnermann, "Multi-gigawatt ultrashort pulses at high repetition rate and average power from two-stage nonlinear compression," Opt. Express **19**, 7546–7552 (2011).
21. V. Cardin, N. Thiré, S. Beaulieu, V. Wanie, F. Légaré, and B. E. Schmidt, "0.42 TW 2-cycle pulses at 1.8 μm via hollow-core fiber compression," Appl. Phys. Lett. **107**, 181101 (2015).
22. Y. Li, H. Zhong, J. Yang, S. Wang, and D. Fan, "Versatile backconversion-inhibited broadband optical parametric amplification based on an idler-separated QPM configuration," Opt. Lett. **42**, 2806–2809 (2017).
23. G. Cerullo and S. D. Silvestri, "Ultrafast optical parametric amplifiers," Rev. Sci. Instrum. **74**, 1–18 (2003).
24. B. W. Mayer, C. R. Phillips, L. Gallmann, and U. Keller, "Mid-infrared pulse generation via achromatic quasi-phase-matched OPCPA," Opt. Express **22**, 20798–20808 (2014).
25. C. R. Phillips, B. W. Mayer, L. Gallmann, and U. Keller, "Frequency-domain nonlinear optics in two-dimensionally patterned quasi-phase-matching media," Opt. Express **24**, 15940–15953 (2016).
26. B. E. Schmidt, N. Thire, M. Boivin, A. Laramee, F. Poitras, G. Lebrun, T. Ozaki, H. Ibrahim, and F. Légaré, "Frequency domain optical parametric amplification," Nat. Commun. **5**, 3643 (2014).
27. D. Brida, C. Manzoni, G. Cirmi, M. Marangoni, S. Bonora, P. Villoresi, S. D. Silvestri, and G. Cerullo, "Few-optical-cycle pulses tunable from the visible to the mid-infrared by optical parametric amplifiers," J. Opt. **12**, 013001 (2010).
28. N. Demirdoven, M. Khalil, O. Golonzka, and A. Tokmakoff, "Dispersion compensation with optical materials for compression of intense sub-100-fs mid-infrared pulses," Opt. Lett. **27**, 433–435 (2002).
29. H. Zhong, L. Zhang, Y. Li, and D. Fan, "Group velocity mismatch-absent nonlinear frequency conversions for mid-infrared femtosecond pulses generation," Sci. Rep. **5**, 10887 (2015).
30. O. Prakash, H. H. Lim, B. J. Kim, K. Pandiyan, M. Cha, and B. K. Rhee, "Collinear broadband optical parametric generation in periodically poled lithium niobate crystals by group velocity matching," Appl. Phys. B **92**, 535–541 (2008).
31. Q. Zhang, E. J. Takahashi, O. D. Mucke, P. Lu, and K. Midorikawa, "Dual-chirped optical parametric amplification for generating few hundred mJ infrared pulses," Opt. Express **19**, 7190–7212 (2011).
32. Y. Fu, E. J. Takahashi, Q. Zhang, P. Lu, and K. Midorikawa, "Optimization and characterization of dual-chirped optical parametric amplification," J. Opt. **17**, 124001 (2015).
33. Y. Fu, E. J. Takahashi, and K. Midorikawa, "High-energy infrared femtosecond pulses generated by dual-chirped optical parametric amplification," Opt. Lett. **40**, 5082–5085 (2015).

34. O. E. Martinez, "Grating and prism compressors in the case of finite beam size," J. Opt. Soc. Am. B **3**, 929–934 (1986).
35. K. Zhao, H. Zhong, P. Yuan, G. Xie, J. Wang, J. Ma, and L. Qian, "Generation of 120 GW mid-infrared pulses from a widely tunable noncollinear optical parametric amplifier," Opt. Lett. **38**, 2159–2161 (2013).
36. X. P. Hu, P. Xu, and S. N. Zhu, "Engineered quasi-phase-matching for laser techniques [Invited]," Photon. Res. **1**, 171–185 (2013).
37. O. Gayer, Z. Sacks, E. Galun, and A. Arie, "Temperature and wavelength dependent refractive index equations for MgO-doped congruent and stoichiometric $LiNbO_3$," Appl. Phys. B **91**, 343–348 (2008).
38. J. Moses and S. W. Huang, "Conformal profile theory for performance scaling of ultrabroadband optical parametric chirped pulse amplification," J. Opt. Soc. Am. B **28**, 812–831 (2011).
39. A. C. Tien, S. Backus, H. Kapteyn, M. Murnane, and G. Mourou, "Short-pulse laser damage in transparent materials as a function of pulse duration," Phys. Rev. Lett. **82**, 3883–3886 (1999).
40. S. A. Rezvani, Q. Zhang, Z. Hong, and P. Lu, "Tunable broadband intense IR pulse generation at non-degenerate wavelengths using group delay compensation in a dual-crystal OPA scheme," Opt. Express **24**, 11187–11198 (2016).
41. C. Wang, Y. Leng, B. Zhao, Z. Zhang, and Z. Xu, "Extremely broad gain spectra of two-beam-pumped optical parametric chirped-pulse amplifier," Opt. Commun. **237**, 169–177 (2004).
42. H. Ishizuki and T. Taira, "Half-joule output optical-parametric oscillation by using 10-mm-thick periodically poled Mg-doped congruent $LiNbO_3$," Opt. Express **20**, 20002–20010 (2012).
43. G. Cerullo, A. Baltuska, O. D. Mucke, and C. Vozzi, "Few-optical-cycle light pulses with passive carrier-envelope phase stabilization," Laser Photon. Rev. **5**, 323–351 (2011).
44. A. Sell, A. Leitenstorfer, and R. Huber, "Phase-locked generation and field-resolved detection of widely tunable terahertz pulses with amplitudes exceeding 100 MV/cm," Opt. Lett. **33**, 2767–2769 (2008).
45. K. L. Vodopyanov, M. M. Fejer, X. Yu, J. S. Harris, Y.-S. Lee, W. C. Hurlbut, V. G. Kozlov, D. Bliss, and C. Lynch, "Terahertz-wave generation in quasi-phase-matched GaAs," Appl. Phys. Lett. **89**, 141119 (2006).
46. F. Junginger, A. Sell, O. Schubert, B. Mayer, D. Brida, M. Marangoni, G. Cerullo, A. Leitenstorfer, and R. Huber, "Single-cycle multiterahertz transients with peak fields above 10 MV/cm," Opt. Lett. **35**, 2645–2647 (2010).